Heliyon 8 (2022) e12329

Contents lists available at ScienceDirect

Heliyon

journal homepage: www.cell.com/heliyon

Research article

The roles of heteromorphic crystals and organic compounds in the formation of the submandibular stones

Zhe Yuan [a,b], Wei-Xin Cai [a,b], Qian Tao [a,b,*]

[a] Hospital of Stomatology, Guanghua School of Stomatology, Sun Yat-sen University, Guangzhou 510080, China
[b] Guangdong Provincial Key Laboratory of Stomatology, Guangzhou 510080, China

ARTICLE INFO

Keywords:
Submandibular stones
Mechanism of formation
Apatite
Biomineralization
Crystal structure
Organic compounds

ABSTRACT

Objective: The study aimed to analyze the formation process of submandibular stones based on the theory of biological mineralization and inorganic crystal structure variation.

Study design: From January 2021 to December 2021, patients with submandibular stones treated in the Affiliated Hospital of Stomatology, Sun Yat-sen University (Guangzhou, China) were selected. According to the criterion of maximum transverse diameter ≥3 mm, a total of five submandibular stones meeting the requirement were included. After the surface of sample stones were washed, they were cut along the maximum transverse diameter. Next, the study employed Scanning Electron Microscope (SEM), Energy Dispersive X-ray Spectroscopy (EDS), and polycrystalline X-ray Diffraction (XRD) to analyze the composition and structure of submandibular stones.

Results: Five submandibular stones were included. The organic and inorganic compounds showed a rhythmic or irregular distribution. Submandibular stones were highly occupied with carbon (C), oxygen (O), calcium (Ca), and phosphorus (P). Hydroxyapatite (HAP) was the primary inorganic component. In addition, the precursor of HAP, namely Amorphous Calcium Phosphate (ACP), was also found. Tetrahedral Substitution Index (TSI) and Ca/P ratio reflected the degree of structural variation in HAP crystal, which fluctuated from 5.62-90.71 and 1.10–1.35, respectively.

Conclusions: The development of submandibular stones was influenced by inorganic crystals' chemical and structural variation as well as the organics' regulation towards the inorganic. The isomorphic substitution was accompanied by the occurrence of inorganic crystals, resulting in the crystal structure change. Organics might influence the appearance, aggregation, and mineralization of HAP during its formation.

1. Introduction

Sialolithiasis is a common non-neoplastic disease characterized by the development of calcified products in salivary glands, especially in the submandibular gland. Patients often have swelling and pain in the affected gland, and recurrent attacks and/or secondary infections can lead to salivary gland dysfunction (Zenk et al., 2012; Galli et al., 2021).

Although exogenous factors such as foreign bodies (Xie et al., 2014b), bacteria (De Grandi et al., 2019), inflammatory cells (Schapher et al., 2020), and endogenous factors such as glandular anatomy and secretion are suggested to be associated with submandibular stones' formation, the exact mechanism remains unclear. From these suggested factors, foreign bodies are rarely observed in the ducts and stones of the submandibular gland (Yu et al., 2010, 2013). Additionally, infection status is not clearly associated with the appearance of stones (Buch et al., 2015). Furthermore, there was no significant difference in the structure of the dominant duct between patients with submandibular stones and healthy controls (Drage et al., 2002). Also, a new perspective on the formation of submandibular stones is urgently needed.

Like stones in other parts of the body, submandibular stones can essentially be considered pathologically mineralized products. Therefore, studying submandibular stone composition and structure can help explain the formation mechanism through biomineralization formation theory.

Submandibular stones are composed of inorganic and organic substances, such as Hydroxyapatite (HAP), Whitlockite (WI), and Brushite (BR) which are the main inorganic compositions among which HAP occupies the majority (Sakae et al., 1981). Due to the complexity of substances in body fluid and the flexibility of the HAP structure, the chemical composition of HAP shows the phenomenon of isomorphism

* Corresponding author.
E-mail address: taoqian@mail.sysu.edu.cn (Q. Tao).

https://doi.org/10.1016/j.heliyon.2022.e12329
Received 1 June 2022; Received in revised form 17 October 2022; Accepted 5 December 2022

substitution. The isomorphism substitution results from other ions partly occupying the positions of certain ions, atoms or molecules in mineral crystals due to similar properties, eventually causing changes in minerals' chemical constitution and crystal structure (Ismail et al., 2017; Liu et al., 2013). Hydrogen (H), oxygen (O), calcium (Ca), and phosphorus (P) are the main elements of standard HAP, but saliva also contains carbon (C), sodium (Na), and magnesium (Mg). They are presented as single ions or chemical groups, having the ability to produce the phenomenon of isomorphism substitution. Therefore, understanding the environment attributed to stones production and the crystal structure of HAP can help us analyze the formation of minerals in submandibular stones.

In addition, organic matters commonly found in humans, such as proteins, polysaccharides and lipids, have the ability to influence inorganic particles aggregation and control mineralizing process (Robin et al., 2021; Sa et al., 2014). Organic compounds are also detected in submandibular stones (Kraaij et al., 2014), but whether they are involved in the mineralization process, and their specific effects on stone formation remains to be further investigated.

This study employed Scanning Electron Microscopy (SEM), Energy Dispersive X-ray Spectroscopy (EDS), and polycrystalline X-ray Diffraction (XRD) to obtain submandibular stones' internal morphology, chemical composition, and crystal parameters, respectively. Notably, this study aimed to identify biomineralization and use the Tetrahedral Substitution Index (TSI) and the Ca/P ratio to demonstrate the involvement of homogeneous substitution in the formation of inorganic compounds in submandibular stones. Furthermore, we searched for evidence of the presence of organic matters in sample stones and tried to explain the effects during the formation of submandibular stones.

2. Materials and methods

2.1. Samples inclusion

With the ethics committee's approval (No.KQEC-2022-37-01), data was collected from patients with submandibular stones at the Affiliated Hospital of Stomatology, Sun Yat-sen University from January 2021 to December 2021. Firstly, the inclusion criteria of patients were as follows: 1) Patients with submandibular stones had complete clinical diagnosis and treatment records and auxiliary examination data; 2) Age of patients $\geq$18 years old; 3) Patients had no previous history of salivary gland disease or radiotherapy for the head and neck; 4) Submandibular stones were entirely removed under general anesthesia in the operating room. Furthermore, the size of sample stones was restricted in order to facilitate the samples' cutting.

Preoperatively, patients' Cone Beam Computed Tomography (CBCT) data were analyzed by RadiAnt DICOM Viewer 25.0 software. Firstly, the definitions of maximum transverse diameter and maximum longitudinal diameter were proposed. The maximum transverse diameter refers to the maximum width of the stone along the ductal cross-section in the coronal section of CBCT, and the maximum longitudinal diameter refers to the maximum length of the stone along the long axis of the duct in the horizontal section of CBCT (Huang et al., 2022). Once removed, stones were washed with saline and distilled water, respectively, and left to dry naturally. Next, submandibular stones were measured using vernier caliper. Based on the preliminary experiments, the maximum transverse diameter $\geq$3 mm was finally selected as the inclusion criteria for stone samples, and samples were cut along the maximum transverse diameter.

2.2. SEM

The central and peripheral stones' regions were analyzed using a field emission SEM (TESCAN MIRA3, Czech Republic) (Im et al., 2017; Tretiakow et al., 2020). After the samples were carbon-coated, SEM images were acquired under an acceleration voltage of 10 kV, a beam current of 15 nA, and a magnification of 300–500x. Due to the small field of view, some images were presented as mosaics of multiple SEM images.

2.3. Elemental analysis

EDS (Quanta 400F, France) was used to analyze the elemental composition with an acceleration voltage of 20 kV (Im et al., 2017). The samples' central and peripheral regions were first identified, and three test areas were selected separately.

2.4. Analysis of inorganic matters

Crystal parameters were analyzed based on XRD analysis. Specifically, an X-ray diffractometer (PANalytical, Netherlands) was utilized with a voltage of 40 kV and an operating current of 40 mA (Kasaboglu et al., 2004; Teymoortash et al., 2003). Samples were scanned with an angle of 20°–80° at a speed of 0.026°/s. Then, the mineral species and crystalline phases were determined using JADE 6.5 software combined element results. The diffraction line spectra were plotted using Origin 2019b software.

2.5. Data analysis

The obtained data were statistically analyzed using SPSS 25.0 software (IBM Corporation, Armonk, NY, USA). The data of each group were firstly tested for normality. The t-test was used for comparison between groups if the data were in line with normal distribution, and Spearman rank correlation analysis was used for comparison between groups if the data were not compliant. All p values <0.05 were defined as significant.

3. Results

3.1. Clinical data of sample cases

Five samples were obtained from five patients with submandibular duct stones. Table 1 shows their basic clinical information. All patients were female, the youngest was 23 years old, and the oldest was 70 years old, with an average age of 51.8. Two patients had a stone in the left submandibular duct and three in the right duct.

The size of sample stones significantly varied. The largest stone was No. 3, having a maximum transverse diameter of 14.56 mm and a maximum longitudinal diameter of 16.49 mm. In contrast, the smallest stone was No.1, having a maximum transverse diameter of 3.00 mm and a maximum longitudinal diameter of 5.25 mm. On average, the maximum transverse diameter was 6.80 mm, and the maximum longitudinal diameter was 9.54 mm.

3.2. Morphology features

Figure 1 shows the morphological features of the samples. The overall profile view of samples could be divided into bright and dark areas according to the brightness difference. The bright and dark bands of samples No.1, No.2, and No.3 were alternately distributed, showing a

Table 1. Patient characteristics.

NO.	Sex	Age(y)	Occurrence site	Number	Size
1	Female	70	Right duct	1	3.00 × 5.25
2	Female	23	Left duct	1	6.10 × 6.15
3	Female	57	Right duct	1	14.56 × 16.49
4	Female	56	Right duct	1	4.41 × 12.67
5	Female	53	Left duct	1	5.95 × 7.13

Stone size: maximum transverse diameter × maximum longitudinal diameter, unit: mm.

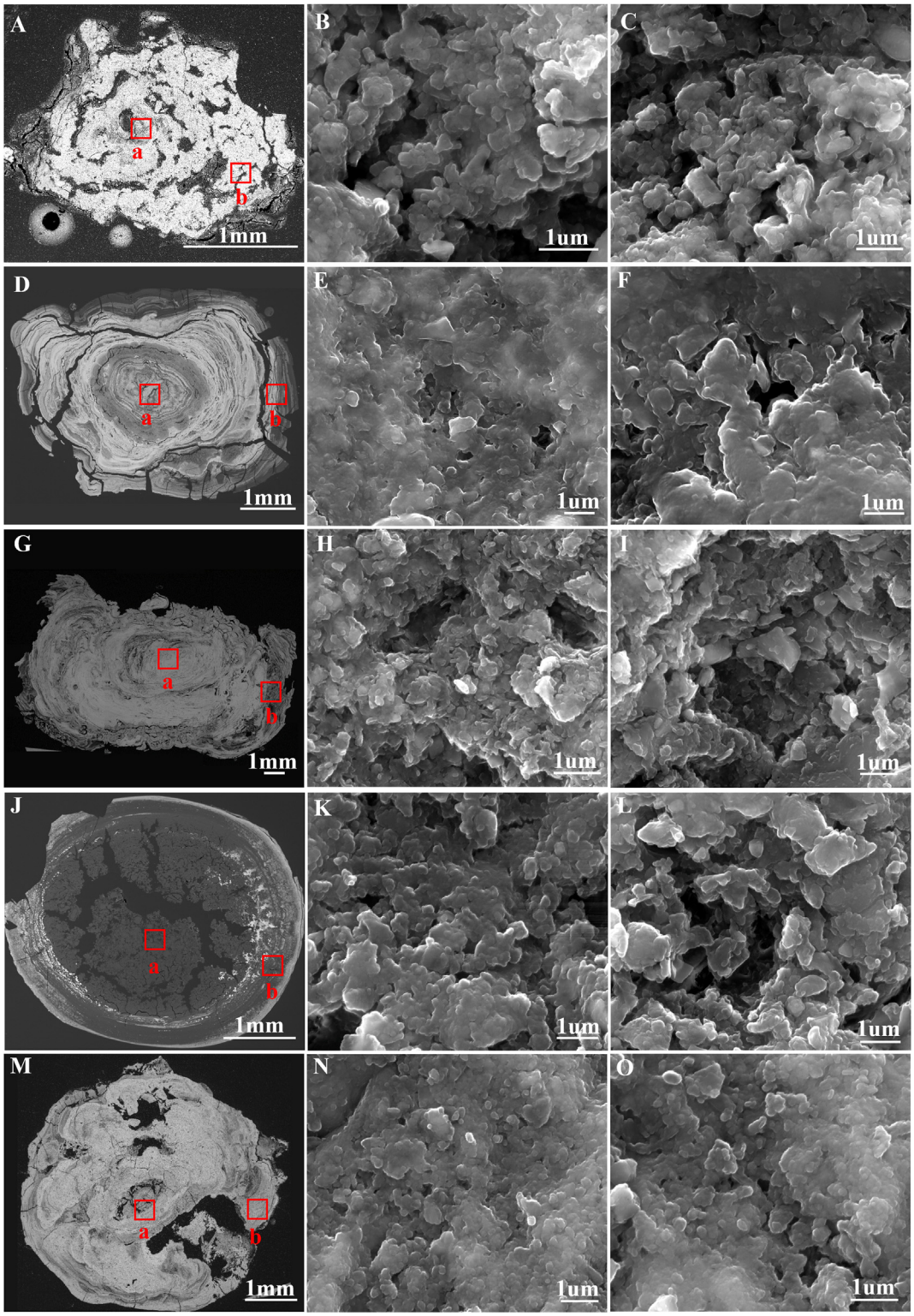

Figure 1. SEM images of five samples. A, D, G, J, and M. Overall profiles (BSE images) of samples No.1-5, respectively. B, E, H, K, and N are magnified views (SE images) of the region "a" in the five samples; C, F, I, L, and O are magnified views (SE images) of the region "b" in the five samples. SEM: Scanning Electron Microscopy, BSE : Backscattering Electron, SE: Secondary Electron.

laminar arrangement (Figure 1A, D, and G), notably No.2 and No.3. No.4 and No.5 were irregularly shaped (Figure 1J and M). No.4 was characterized as having a dark area in the center and part of the peripheral area, while No.5 was mainly characterized by an evenly distributed bright area. Furthermore, magnified images observed spherical particles (Figure 1B, C, E, F, H, I, K, L, N, and O), most of which fused to form clumped structures with interspaces between them.

3.3. Elements composition

Element types and relative contents of stone samples are shown in Table 2. C, O, Ca and P composed the majority of elements in five cases, accounting for 98.77%, 99.37%, 99.18%, 99.17% and 98.83% on average, respectively, while the contents of Na, Mg, silicon (Si), sulphur (S), chlorine (Cl) and potassium (K) were minimal.

Table 2. Element analysis of samples.

Kind	1		2		3		4		5	
	CEN	PER	CEN	PER	CEN	PER	CEN	PER	CEN	PER
C	38.40	58.76	35.41	46.86	23.26	46.51	40.70	71.07	33.52	41.16
O	49.60	35.51	49.93	42.22	50.42	38.69	46.39	26.73	48.82	45.26
Ca	5.43	2.66	7.75	5.96	14.73	8.05	6.33	0.74	8.40	7.21
P	4.89	2.27	6.19	4.41	10.63	6.06	5.71	0.67	7.58	5.73
Na	0.60	0.33	0.33	0.32	0.48	0.39	0.29	0.21	0.50	0.19
Mg	0.19	0.07	0.16	0.07	0.30	0.12	0.32	0.02	0.60	0.30
Si	0.75	0.33	-	0.04	-	-	-	0.08	0.47	0.09
S	0.03	0.01	0.15	0.05	0.06	0.03	0.19	0.42	-	-
Cl	0.07	0.06	0.10	0.06	0.13	0.15	0.07	0.05	0.11	0.05
K	0.04	-	-	-	-	-	-	-	0.02	-

Relative content was calculated based on atomic number (%).
Abbreviations: CEN: center, PER: periphery, C: carbon, O: oxygen, Ca: calcium, P: phosphorus, Na: sodium, Mg: magnesium, Si: silicon, S: sulphur, Cl: chlorine, K: potassium.

3.4. Inorganic compounds

Figure 2 shows five samples' line spectra based on XRD results. Sample No. 3 had a relatively high degree of crystallization, because several highly picked diffraction peaks were observed. In contrast, other samples' overall identification was low, primarily samples No. 1 and No. 4. The diffraction patterns of all samples revealed the broad and short crystal packages in the range of 30°–33°.

Combined with the elemental species and relative contents obtained from EDS, it was possible to infer the composition of inorganic compounds in submandibular stones. The samples tested in this study mainly consisted of HAP, WI, and BR. Figure 2A shows the comparison of the sample with the HAP diffraction results. The diffraction curves of the five sample stones exhibited varied intensity at 31.74°, where the signature HAP peak (211) is located. Samples No.2, No.3, and No.5 also corresponded to other signature peaks. Next, No.2-5 expressed a small amount of weak WI signal compared with the standard WI profile, while No.1 failed to show any patterns (Figure 2B). Figure 2C compares the diffraction data of the samples with the standard BR profile, and only one low peak was apparent at 47.8° in No.3.

3.5. Analysis of the variability of inorganic crystal structures

Phase analysis indicated that HAP mainly occupied inorganic matters. However, in addition to the basic elements that constituted HAP, the samples also contained a large amount of C and trace elements such as Na, K, and Mg, and these elements could participate in the replacement of the HAP chemical structure (Figure 3). This study used TSI and Ca/P values to illustrate the variation degree of inorganic crystals.

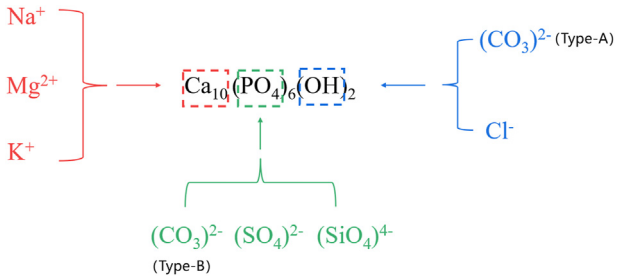

Figure 3. Isomorphism substitution of HAP. HAP: Hydroxyapatite.

3.6. TSI values

TSI = (Si + S + C)/P ×100 (Stoppa and Yu, 1995)

TSI values are shown in Table 3. No.1 had the largest TSI value with an average of 90.71, and No.3 had the smallest TSI value with an average of 5.62. In five samples, TSI values in the central area were lower than that in the peripheral area, but the difference was not statistically significant.

3.7. Ca/P values

Table 4 lists Ca/P values in different regions of sample stones. No.1 was the lowest, with an average of 1.10, and sample No.3 was the highest, with an average of 1.35. There was no statistical difference between the center and the peripheral area in the samples.

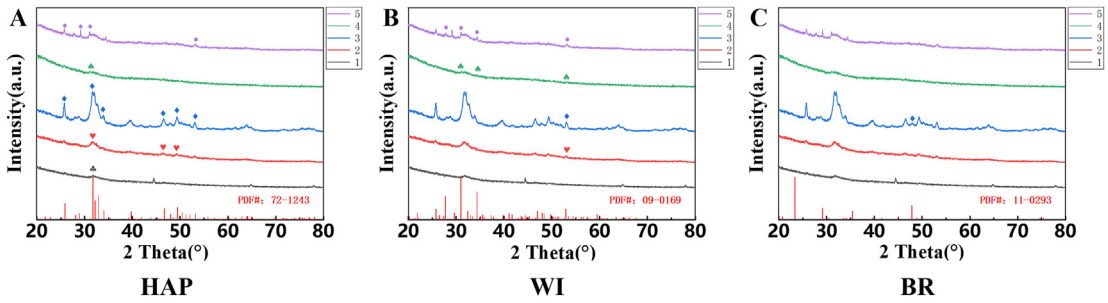

Figure 2. XRD analysis of five samples. A, B, and C represent diffraction peaks of the five samples, compared with the standard PDF of hydroxyapatite, whitlockite, and brushite, respectively. XRD: X-ray Diffraction, HAP: Hydroxyapatite, WI: Whitlockite, BR: Brushite. "♧、♥、◇、♤、○" marked the peak values of corresponding standard spectra on XRD line spectra of No.1-5, respectively. The standard PDF card numbers for comparison for HAP, WI, and BR were 72–1243, 09–0169, and 11–0293, respectively.

Table 3. Statistical analysis of TSI.

No.	CEN		PER		mean	t value	*p* value
	mean	SD	mean	SD			
1	8.13	1.39	173.29	180.04	90.71	-1.59	0.187
2	5.93	1.62	15.11	13.52	10.52	-1.17	0.361
3	2.24	0.82	9.00	5.24	5.62	-2.21	0.092
4	7.50	2.62	152.48	106.88	79.99	-2.35	0.079
5	4.60	1.79	7.38	2.00	5.99	-1.79	0.147

Abbreviations: TSI: Tetrahedral Substitution Index, CEN: center, PER: periphery, SD: standard deviation.

4. Discussion

Based on the research methods and formation theories of common human body stones (such as gallstones, kidney stones and dental pulp stones) and natural apatite minerals, we explored the formation mechanism of submandibular stones (Chatterjee et al., 2018; Milcent et al., 2019; Peter et al., 2020). This study introduced the theory of biomineralization and inorganic crystal variation to explain the formation mechanism of submandibular stones based on their composition, structure, and morphology. Five patients with submandibular stones were included as the source of stone samples. The profile morphology of the stones in the samples showed rhythmic or irregular structure, which was also consistent with previous report (Tretiakow et al., 2020). Additionally, structure analysis suggested sample stones were mainly composed of HAP. Furthermore, composition analysis showed that submandibular stones still contained C, Na, Mg, Si, S, Cl and K, in addition to the basic elements of HAP crystals. Therefore, these findings suggest isomorphism substitution phenomenon in HAP crystals in submandibular stones, leading to structural changes. What's more, we also concerned about the potential role of organics in submandibular stones formation.

4.1. Clinical features of submandibular stones

Combined with typical clinical symptoms with auxiliary examinations such as CBCT, ultrasound, and sialoendoscopy, most patients with submandibular stones can be accurately diagnosed (Schwarz et al., 2015). Additionally, minimally invasive stone extraction is an effective treatment for relieving obstructive symptoms in patients, in which most patients regain salivary flow and improve glandular function shortly after stone removal. However, long-term follow-up studies suggested a risk of recurrence. Three studies followed patients with submandibular stones after stone extraction with a mean time of 19.8 months, 54.8 months, and 42 months, respectively. They found that all three study groups experienced varied degrees of recurrence, with recurrence rates fluctuating from 3.39 % to 10.4 %, and one patient even had a second recurrence of stones (Galli et al., 2021; Kim et al., 2016; Zhang et al., 2010). The recurrent patients bear a greater risk of gland removal than the first therapy (Galli et al., 2021).

Table 4. Statistical analysis of Ca/P.

No.	CEN		PER		mean	t value	*p* value
	mean	SD	mean	SD			
1	1.11	0.10	1.10	0.12	1.10	0.07	0.946
2	1.24	0.10	1.29	0.18	1.27	-0.45	0.676
3	1.38	0.03	1.32	0.05	1.35	1.82	0.143
4	1.10	0.19	1.12	0.06	1.11	-0.21	0.848
5	1.11	0.08	1.24	0.30	1.18	-0.72	0.514

Abbreviations: Ca: calcium, P: phosphorus, CEN: center, PER: periphery, SD: standard deviation.

The ideal disease diagnosis and treatment state is to prevent it and reduce the number of patients entering the clinical stage, and understanding the disease development is the primary aspect of prevention. The formation mechanism of submandibular stones has not been fully elucidated yet, which hinders the preclinical treatment (Sigismund et al., 2015). Submandibular stones are biominerals and form under an environment similar to common human hard tissues such as teeth and bones. Submandibular stones' composition and structure can reflect the formation process.

4.2. Biomineralization and formation of submandibular stones

Biomineralization refers to the formation of structurally diverse and functionally specific minerals under the control of organic matter and biomolecules in living organisms (Mann, 2005). Biomineralization products are called biominerals, which are organic-inorganic complexes with specific orientations and complex structures (Sharma et al., 2021). Biominerals are divided into two main groups: calcified biominerals and non-calcified biominerals. The former is mainly composed of carbonates and phosphates, such as human bones and teeth, and the latter is mainly in the form of silicide (Gower, 2008). Vitro nucleation kinetic studies have confirmed that HAP formation requires three stages: induction, crystallization, and maturation. In simulated body fluids, Ca and P form precursor substances, mainly ACP, representing the appearance of the induction phase. Following the induction phase, the pH decreases. Finally, the crystallization maturation phase is reached once the pH stabilizes (Chen et al., 2014; Xie et al., 2014a). The simplified chemical equation of above transformation process is as follows :

$3Ca_3(PO_4)_2(s) + Ca^{2+} + 2H_2O \rightarrow 2Ca_5(PO_4)_3(OH)\ (s) + 2H^+$ (Jiang et al., 2021)

From the XRD results, no obvious diffraction peaks were observed in any samples at an angle of 30° at 2θ, indicating the existence of ACP (Vecstaudza et al., 2019). The presence of ACP suggests that the formation of inorganic crystals in the submandibular stones undergoes transformation of precursor substances.

4.3. Crystal chemistry and variation structure analysis

Under SEM fields, particles were the basic units making up submandibular stones. According to XRD results, most particles mainly contained HAP. They were spherical in shape and fused to each other. The mature HAP crystals are slightly rounded and hexagonal, and the spherical morphology suggests poor crystallinity and mineralization (Kasaboglu et al., 2004). The basic elements of apatite are H, O, Ca, and P. However, EDS did not detect H because of the lightest mass and the smallest atomic number in all chemical elements and its unstable property. The absence of H in the study did not mean that it was not presented in submandibular stones. In addition, a large amount of C and trace amounts of Na, K, and Mg were detected in sample stones, potentially replacing certain chemical compounds in HAP, leading to the variation in the crystal structure.

The basic chemical formula of HAP is $Ca_{10}(PO_4)_6(OH)_2$. The type and number of substitutions affect the degree of variability of inorganic crystals (Cacciotti, 2019). Generally, $(PO_4)^{3-}$ is a tetrahedral structure with a negative trivalent. Although $(PO_4)^{3-}$ has the same tetrahedral structure as $(CO_3)^{2-}$, $(SO_4)^{2-}$, and $(SiO_4)^{4-}$, these replacements make the tetrahedra distorted because of the different charges carried by the groups, with $(CO_3)^{2-}$ causing the most significant degree of distortion, known as substitution type-B (Comodi and Liu, 2000). In addition, Na, K, and Mg are able to participate in the Ca^{2+} site substitution in the form of Na^+, K^+, and Mg^{2+}, respectively. The participation of Na^+ and K^+ in the Ca^{2+} site does not significantly affect the crystallinity, but Mg^{2+} substitution causes a decrease in the crystallinity of HAP (Ibsen et al., 2016). Since the average percentage of the three elements in this analysis was extremely low and not detectable at some sites, it is reasonably presumed

that the main site causing the structural variation of HAP in the sample stones is not the Ca^{2+} position. Cl in sample stones can occupy the original (-OH) position. However, the overall HAP structure is less affected by Cl^{-} substitution (John et al., 1989). $(CO_3)^{2-}$ is also capable of occupying the (-OH) position, namely type A substitution, yet it is rare in biogenic mineralization (Hughes et al., 2019; Pasteris et al., 2008).

This finding showed that the primary location where HAP substitution occurred in submandibular stones was at the $(PO_4)^{3-}$ position. To describe the degree of replacement, we firstly employed TSI value to analyze the variation degree of $(PO_4)^{3-}$. When no substitution occurs, the value is 0 according to the calculation formula. From our observations, the mean TSI value of the five submandibular stones fluctuated from 5.62 to 90.71, suggesting that the isomorphic substitution and structural variation occur in HAP crystals. In addition, the TSI value is of great significance for predicting the origin of apatite. In this study, compared with S and Si, the content of C had an absolute advantage, which played a critical role in TSI value. It has been confirmed that the structural replacement of large amounts of $(CO_3)^{2-}$ can improve the formation rate of HAP in vitro simulation experiment (Gibson and Bonfield, 2002). Hence, it is reasonable to speculate that $(CO_3)^{2-}$ plays a promoting role in the formation and progression of submandibular stones. However, due to the presence of organic matter, the C content of the samples did not fully reflect the extent of $(CO_3)^{2-}$ involvement in the formation of HAP. Notably, the TSI values in the study were less than the calculated values.

Ca^{2+} and $(PO_4)^{3-}$ play an important role in the final mineral types, the metal ion available for replacement in these samples is extremely low, and the main replacement location is the $(PO_4)^{3-}$ site. Therefore, Ca/P values can reflect the degree substitution phenomenon. The replacing elements were not involved in the calculating process, which avoided the deviation caused by organic elements. Ca/P values in the study were lower than the standard value (1.67). The replacement of $(PO_4)^{3-}$ causes the ratio to decrease. Furthermore, the decrease in Ca/P value weakens the crystallinity of HAP in the submandibular stones, which is one of the reasons for the poor quality of diffraction patterns. We found that the standard crystallinity of HAP is 74.3%. As noted from previous study, when Ca/P value drops to 1.50, 1.20 and 1.10, the crystallinity is 65.8%, 60.5% and 52.2%, respectively (Huang et al., 2001).

HAP synthesis requires the transition of multiple intermediates in vitro, also known as the transition between multiple phases. Common phases include ACP, Octacalcium Phosphate (OCP), and Tertiary Calcium Phosphate (TCP), and the relative contents of Ca^{2+} and $(PO_4)^{3-}$ in these matters are different from the standard HAP. Therefore, the Ca/P values could be used to appropriately predict the presence of HAP precursor components in submandibular stones (Johnsson and Nancollas, 1992; Wang and Nancollas, 2008). The Ca/P ratio for ACP fluctuates between 1.2 and 2.2, whereas it for OCP and TCP is 1.33 and 1.50, respectively (Dorozhkin and Epple, 2002). The average Ca/P value of the tested samples fluctuated from 1.10 to 1.35, suggesting that HAP precursor substances may exist in submandibular stones. Therefore, this may be a reason for the poor identification of XRD results.

4.4. Potential effects of organic compounds

BSE (Backscattering Electron) and SE (Secondary Electron) imaging methods were used in this analysis during SEM observation. BSE images could not only observe the overall morphology of stone samples at a lower magnification ratio but also reflected the overall chemical composition of stone samples. SE images were used since local magnification images paid more attention to the structure of basic constituent units of samples (Saghiri et al., 2012). Under BSE conditions, the luminance difference is caused by the atomic number difference. Notably, with an increasing atomic number, the brightness also gradually increases (Sanchez et al., 2012). According to EDS results, C, O, P, and Ca mainly occupied submandibular stones. The atomic numbers of C and O are 6 and 8, respectively, while the atomic numbers of P and Ca rise to 15 and 20, respectively. The bright area contains more P and Ca, which are the main elements of apatite, and the dark area is mainly composed of C and O. It is reasonable to expect that HAP dominates the bright area, and the dark area indicates a large amount of organic matter (Tretiakow et al., 2021).

Organic molecules can offer a framework for biomineralization, provide sites for the generation of inorganic materials, and control crystal growth. A study analyzed the protein composition in 29 cases of salivary stones, with the maxilla as control. A total of 6,934 kinds of protein were detected by liquid chromatography-mass spectrometry (LC-MS) (Busso et al., 2020). The protein contained in salivary stones has a certain homology with bone morphogenetic protein, with an average of 53%. Subsequently, functional analysis demonstrated that extracellular exosomes (EE) play an essential role.

Organics can provide the initial framework for the deposition of inorganic minerals and affect the regulation of salt deposition and inorganic mineral crystal morphology. Under the regulation template of chitosan-polylactic acid, the crystalline phase of HAP was limited (Cai et al., 2009, 2011). Boda et al. (2019) added Bone Morphogenetic Protein 2 (BMP-2) to mineralized fiber skeleton in vitro to analyze its effect on the osteogenic ability of alveolar bone. After four weeks, the results showed that the volume and density of alveolar bone in the experimental group increased by 3 times compared with the control group. In addition, organic matters have positive or negative regulatory effects on the formation of teeth. Soluble proteins, lipids, polysaccharides as well as other common organic substances in the human body promote the generation and mineralization of enamel and dentin, while the clock protein Rev-ERBs interferes with the mineralization of cementum (Fu et al., 2022).

While the formation mechanism of submandibular stones needs to be further explored and verified, simply preventive ways may help reduce the rate of occurrence of submandibular stones. Compared with healthy people, the mineral ion concentration of mixed saliva or submandibular gland fluid of patients with submandibular stones has significant changes, especially the concentration of Ca^{2+} is significantly higher than that of normal people, suggesting that reducing the intake of foods rich in Ca may help to inhibit submandibular stones' production (Schroder et al., 2017; Su et al., 2010). In addition, low levels of crystallization inhibitors, such as citrate, phytate, and Mg, are detected in the saliva of patients (Grases et al., 2003; Su et al., 2010). Drinking more water or consuming acidic substances can accelerate saliva secretion and increase the flow of saliva in the ducts, which may help to inhibit crystallization.

A major limitation of our study is the small sample size due to the strict inclusion criteria. Another limitation is the methods we used are basal. The extensibility of results was limited to some extent. Therefore, further work is required to clarify the formation mechanism of submandibular stones in a large-scale cohort study and employ more accurate methods.

In conclusion, inorganic crystals and organic compounds contributed to the generation and development of submandibular stones. The formation of HAP results from the transformation of precursor matters. In addition, it was disturbed by foreign elements in saliva during HAP formation, resulting in chemical structure changes in HAP crystal. Simultaneously, the organic matters may provide the mineralization framework, regulate the accumulation of inorganic minerals, and affect the degree of mineralization of inorganic minerals during the formation of submandibular stones.

Declarations

Author contribution statement

Zhe Yuan: Conceived and designed the experiments; Performed the experiments; Analyzed and interpreted the data; Contributed reagents, materials, analysis tools or data; Wrote the paper.

Wei-Xin Cai: Contributed reagents, materials, analysis tools or data.

Qian Tao: Conceived and designed the experiments; Wrote the paper.

Funding statement

Qian Tao was supported by National Natural Science Foundation of China [81072227].

Data availability statement

Data included in article/supp. material/referenced in article.

Declaration of interest's statement

The authors declare no conflict of interest.

Additional information

No additional information is available for this paper.

Acknowledgements

We thank Miss Chen-Yu Zhang for her help in samples' measurement.

References

Boda, S.K., Almoshari, Y., Wang, H.J., Wang, X.Y., Reinhardt, R.A., Duan, B., Xie, J.W., 2019. Mineralized nanofiber segments coupled with calcium-binding BMP-2 peptides for alveolar bone regeneration. Acta Biomater. 85, 282–293.

Buch, K., Nadgir, R., Fujita, A., Tannenbaum, A., Ozonoff, A., Sakai, O.J.T.L., 2015. Clinical associations of incidentally detected parotid gland calcification on CT. Laryngoscope 125 (6), 1360–1365.

Busso, C.S., Guidry, J.J., Gonzalez, J.J., Zorba, V., Son, L.S., Winsauer, P.J., Walvekar, R.R., 2020. A comprehensive analysis of sialolith proteins and the clinical implications. Clin. Proteonomics 17, 12.

Cacciotti, I., 2019. Multisubstituted hydroxyapatite powders and coatings: the influence of the codoping on the hydroxyapatite performances. Int. J. Appl. Ceram. Technol. 16 (5), 1864–1884.

Cai, X., Tong, H., Shen, X.Y., Chen, W.X., Yan, J., Hu, J.M., 2009. Preparation and characterization of homogeneous chitosan-polylactic acid/hydroxyapatite nanocomposite for bone tissue engineering and evaluation of its mechanical properties. Acta Biomater. 5 (7), 2693–2703.

Cai, X., Chen, L., Shen, X., Hu, J., Tong, H., Jiang, T., 2011. Facile synthesis of anisotropic porous chitosan/hydroxyapatite scaffolds for bone tissue engineering. J. Mater. Chem. 21 (32), 12015–12025.

Chatterjee, P., Chakraborty, A., Mukherjee, A.K., 2018. Phase composition and morphological characterization of human kidney stones using IR spectroscopy, scanning electron microscopy and X-ray Rietveld analysis. Spectrochim. Acta Mol. Biomol. Spectrosc. 200, 33–42.

Chen, Y., Gu, W., Pan, H., Jiang, S., Tang, R., 2014. Stabilizing amorphous calcium phosphate phase by citrate adsorption. CrystEngComm 16 (10), 1864–1867.

Comodi, P., Liu, Y., 2000. CO3 substitution in apatite: further insight from new crystal-chemical data of Kasekere (Uganda) apatite. Eur. J. Mineral 12 (5), 965–974.

De Grandi, R., Capaccio, P., Bidossi, A., Bottagisio, M., Drago, L., Torretta, S., De Vecchi, E., 2019. Salivary calculi microbiota: new insights into microbial networks and pathogens reservoir. Microb. Infect. 21 (2), 109–112.

Dorozhkin, S.V., Epple, M., 2002. Biological and medical significance of calcium phosphates. Angew. Chem. Int. Ed. 41 (17), 3130–3146, 2-1.

Drage, N.A., Wilson, R.F., McGurk, M., 2002. The genu of the submandibular duct–is the angle significant in salivary gland disease? Dentomaxillofacial Radiol. 31 (1), 15–18.

Fu, L., Wang, M., Zhu, G., Zhao, Z., Sun, H., Cao, Z., Xia, H., 2022. REV-ERBs negatively regulate mineralization of the cementoblasts. Biochem. Biophys. Res. Commun. 587, 9–15.

Galli, P., Ceva, A., Foletti, J.M., Iline, N., Giorgi, R., Chossegros, C., Graillon, N., 2021. Salivary gland lithiasis recurrence after minimally-invasive surgery: incidence, risk factors and prevention. Laryngoscope 131 (4), 794–799.

Gibson, I.R., Bonfield, W., 2002. Novel synthesis and characterization of an AB-type carbonate-substituted hydroxyapatite. J. Biomed. Mater. Res. 59 (4), 697–708.

Gower, L.B., 2008. Biomimetic model systems for investigating the amorphous precursor pathway and its role in biomineralization. Chem. Rev. 108 (11), 4551–4627.

Grases, F., Santiago, C., Simonet, B.M., Costa-Bauza, A., 2003. Sialolithiasis: mechanism of calculi formation and etiologic factors. Clin. Chim. Acta 334 (1-2), 131–136.

Huang, Z.L., Liu, Y., Wang, D.W., Zhang, S.G., Chen, L.J., 2001. Properties of crystallizing and absorbing F- ion of HAP synthesized by sol-gel process. J. Inorg. Mater. 16 (4), 661–666.

Huang, Y., Liang, P.S., Yang, Y.C., Cai, W.X., Tao, Q., 2022. Nomogram to predict the risk of endoscopic removal failure with forceps/baskets for treating submandibular stones. World J. Clin. Cases 10 (9), 2710–2720.

Hughes, E.A.B., Robinson, T.E., Bassett, D.B., Cox, S.C., Grover, L.M., 2019. Critical and diverse roles of phosphates in human bone formation. J. Mater. Chem. B 7 (47), 7460–7470.

Ibsen, C.J., Chernyshov, D., Birkedal, H., 2016. Apatite Formation from amorphous calcium phosphate and mixed amorphous calcium phosphate/amorphous calcium carbonate. Chemistry 22 (35), 12347–12357.

Im, Y.G., Kook, M.S., Kim, B.G., Kim, J.H., Park, Y.J., Song, H.J., 2017. Characterization of a submandibular gland sialolith: micromorphology, crystalline structure, and chemical compositions. Oral Surg. Oral Med. Oral Path. Oral Radiol. 124 (1), E13–E20.

Ismail, Y.M.B., Wimpenny, I., Bretcanu, O., Dalgarno, K., El Haj, A.J., 2017. Development of multisubstituted hydroxyapatite nanopowders as biomedical materials for bone tissue engineering applications. J. Biomed. Mater. Res. 105 (6), 1775–1785.

Jiang, S.Q., Cao, Y.Y., Zong, C.X., Pang, Y.F., Sun, Z.W., 2021. Appropriate regulation of magnesium on hydroxyapatite crystallization in simulated body fluids. CrystEngComm 23 (3), 678–683.

John, M. Hughes, Cameron, M., Crowley, K., 1989. Structural variations in natural F, OH, and Cl apatites. Am. Mineral. 870–876.

Johnsson, M.S., Nancollas, G.H., 1992. The role of brushite and octacalcium phosphate in apatite formation. Critical reviews in oral biology and medicine. Off. Pub. Am. Assoc. Oral Biol. 3 (1-2), 61–82.

Kasaboglu, O., Er, N., Tumer, C., Akkocaoglu, M., 2004. Micromorphology of sialoliths in submandibular salivary gland: a scanning electron microscope and X-ray diffraction analysis. J. Oral Maxillofac. Surg. 62 (10), 1253–1258.

Kim, J.K., Shin, S.M., Lee, H., Lee, S., 2016. Factors affecting long-term outcome of transoral surgery for submandibular stones: a follow-up study of 125 patients. Clin. Otolaryngol. 41 (4), 365–370.

Kraaij, S., Karagozoglu, K., Forouzanfar, T., Veerman, E., Brand, H.J. B.d. j., 2014. Salivary stones: symptoms. aetiology, biochemical composition and treatment 217 (11), E23.

Liu, Q., Huang, S., Matinlinna, J.P., Chen, Z., Pan, H., 2013. Insight into biological apatite: physiochemical properties and preparation approaches. BioMed Res. Int. 2013, 929748.

Mann, S., 2005. Biomineralization: Principles and Concepts in Bioinorganic Materials Chemistry. Oxford University Press.

Milcent, C.P.F., da Silva, T.G., Baika, L.M., Grassi, M.T., Carneiro, E., Franco, A., de Lima, A.A.S., 2019. Morphologic, structural, and chemical properties of pulp stones in extracted human teeth. J. Endod. 45 (12), 1504–1512.

Pasteris, J.D., Wopenka, B., Valsami-Jones, E., 2008. Bone and tooth mineralization: why apatite? Elements 4 (2), 97–104.

Peter, A., Cozmuta, L.M., Nicula, C., Cozmuta, A.M., Vulpoi, A., Barbu-Tudoran, L., Pop, F.G., 2020. Multi-analyses of gallstones and correlation between their properties with the laboratory results. Anal. Biochem. 593, 13.

Robin, M., Tovani, C.B., Krafft, J.M., Costentin, G., Azais, T., Nassif, N., 2021. The concentration of bone-related organic additives drives the pathway of apatite formation. Cryst. Growth Des. 21 (7), 3994–4004.

Sa, Y., Liang, S., Ma, X., Lu, S., Wang, Z., Jiang, T., Wang, Y., 2014. Compositional, structural and mechanical comparisons of normal enamel and hypomaturation enamel. Acta Biomater. 10 (12), 5169–5177.

Saghiri, M.A., Asgar, K., Lotfi, M., Karamifar, K., Saghiri, A.M., Neelakantan, P., Sheibaninia, A., 2012. Back-scattered and secondary electron images of scanning electron microscopy in dentistry: a new method for surface analysis. Acta Odontol. Scand. 70 (6), 603–609.

Sakae, T., Yamamoto, H., Hirai, G., 1981. Mode of occurrence of brushite and whitlockite in a sialolith. J. Dent. Res. 60 (4), 842–844.

Sanchez, E., Deluigi, M.T., Castellano, G., 2012. Mean atomic number quantitative assessment in backscattered electron imaging. Microsc. Microanal. 18 (6), 1355–1361.

Schapher, M., Koch, M., Weidner, D., Scholz, M., Wirtz, S., Mahajan, A., Herrmann, M., 2020. Neutrophil extracellular traps promote the development and growth of human salivary stones. Cells 9 (9).

Schroder, S.A., Homoe, P., Wagner, N., Bardow, A., 2017. Does saliva composition affect the formation of sialolithiasis? J. Laryngol. Otol. 131 (2), 162–167.

Schwarz, D., Kabbasch, C., Scheer, M., Mikolajczak, S., Beutner, D., Luers, J.C., 2015. Comparative analysis of sialendoscopy, sonography, and CBCT in the detection of sialolithiasis. Laryngoscope 125 (5), 1098–1101.

Sharma, V., Srinivasan, A., Nikolajeff, F., Kumar, S., 2021. Biomineralization process in hard tissues: the interaction complexity within protein and inorganic counterparts. Acta Biomater. 120, 20–37.

Sigismund, P.E., Zenk, J., Koch, M., Schapher, M., Rudes, M., Iro, H., 2015. Nearly 3,000 salivary stones: some clinical and epidemiologic aspects. Laryngoscope 125 (8), 1879–1882.

Stoppa, F., Yu, L., 1995. Chemical composition and petrogenetic implications of apatites from some ultra-alkaline Italian rocks. Eur. J. Mineral 7 (2), 391–402.

Su, Y.X., Zhang, K., Ke, Z.F., Zheng, G.S., Chu, M., Liao, G.Q., 2010. Increased calcium and decreased magnesium and citrate concentrations of submandibular/sublingual saliva in sialolithiasis. Arch. Oral Biol. 55 (1), 15–20.

Teymoortash, A., Buck, P., Jepsen, H., Werner, J.A., 2003. Sialolith crystals localized intraglandularly and in the Wharton's duct of the human submandibular gland: an X-ray diffraction analysis. Arch. Oral Biol. 48 (3), 233–236.

Tretiakow, D., Skorek, A., Ryl, J., Wysocka, J., Darowicki, K., 2020. Ultrastructural analysis of the submandibular sialoliths: Raman spectroscopy and electron back-scatter studies. Ultrastruct. Pathol. 44 (2), 219–226.

Tretiakow, D., Skorek, A., Wysocka, J., Darowicki, K., Ryl, J., 2021. Classification of submandibular salivary stones based on ultrastructural studies. Oral Dis. 27 (7), 1711–1719.

Vecstaudza, J., Gasik, M., Locs, J., 2019. Amorphous calcium phosphate materials: formation, structure and thermal behaviour. J. Eur. Ceram. Soc. 39 (4), 1642–1649.

Wang, L.J., Nancollas, G.H., 2008. Calcium orthophosphates: crystallization and dissolution. Chem. Rev. 108 (11), 4628–4669.

Xie, B.Q., Halter, T.J., Borah, B.M., Nancollas, G.H., 2014a. Tracking amorphous precursor formation and transformation during induction stages of nucleation. Cryst. Growth Des. 14 (4), 1659–1665.
Xie, L., Zheng, L., Yu, C., Yang, C., Chen, Z., Yun, B., Kim, E., 2014b. Foreign body induced sialolithiasis treated by sialoendoscopic intervention. J. Craniofac. Surg. 25 (4), 1372–1375.
Yu, C.Q., Yang, C., Zheng, L.Y., Wu, D.M., 2010. Endoscopic observation and strategic management of obstructive submandibular sialadenitis. J. Oral Maxillofac. Surg. 68 (8), 1770–1775.
Yu, C.Q., Yang, C., Zheng, L.Y., 2013. Sialendoscopic findings in patients with obstructive sialadenitis: long-term experience. Br. J. Oral Maxillofac. Surg. 51 (4), 337–341.
Zenk, J., Koch, M., Klintworth, N., Konig, B., Konz, K., Gillespie, M.B., Iro, H., 2012. Sialendoscopy in the diagnosis and treatment of sialolithiasis: a study on more than 1000 patients. Otolaryngology-Head Neck Surg. (Tokyo) 147 (5), 858–863.
Zhang, L., Escudier, M., Brown, J., Capaccio, P., Pignataro, L., McGurk, M., 2010. Long-term outcome after intraoral removal of large submandibular gland calculi. Laryngoscope 120 (5), 964–966.